ISSN: 2692-5397
DOI: 10.33552/MCMS.2022.04.000599
Modern Concepts in Material Science
Iris Publishers

Research Article



# Investigations on the Time Dependence of the Wetting Behavior of Ceramics by Means of Picosecond Laser Processing

**Michael Seiler*, Klemens Reichelt, Jens Bliedtner**

*Ernst-Abbe-University Jena, Carl-Zeiss-Promenade 2, Germany*

***Corresponding author:** Michael Seiler, Ernst-Abbe-University Jena, Carl-Zeiss-Promenade 2, 07745 Jena, Germany.

**Received Date:** August 22, 2022

**Published Date:** September 08, 2022

## Abstract

Structuring technical ceramics by means of ultrashort-pulsed laser radiation is a promising technology for the formation of pillar and hole structures in the micrometer range. The surface wettability of ceramic substrates can specifically be realized by ultrashort laser pulses (ps) and a galvanometric scanner. The results show that the contact angle of water (WCA) depends on the measurement time point after laser processing. Experimental investigations reveal that laser-structured ceramics like aluminum nitride and aluminum oxide show hydrophilic (<90°) to super hydrophilic (<10°) behavior directly after processing. However, superhydrophobic contact angles CA can be measured with the applied materials 250 days after processing. Besides this temporal influence, structure size, distance and height of the laser-processed substrates play a role in the change of the wetting behavior.

**Keywords:** Time depending water contact angle; Wetting behavior; Ceramic; Laser structuring, Wenzel; Cassie-baxter

## Introduction

The wettability of surfaces is a crucial material characteristic, which mainly depends on the surface's morphology and chemistry [1]. Indicator for the change of the wetting behavior is the contact angle CA and this change, amongst others, results from measuring the static contact angle between a fluid (e.g., distilled water) and the solid boundary surface. Different degrees of wetting can be reached through surface structuring. If the contact angle is narrower than 90°, the surface is hydrophilic. If it is larger than 90°, it is hydrophobic. Hydrophobic as well as hydrophilic surfaces can be generated on many materials such as plastics, metals, ceramics or glass through direct laser irradiation [2-5]. Additionally, there are further technical solutions like mask lighting or etching procedures [2,6-8].

Wettability basically depends on the surface structure. The structuring can be realized in different dimensions (macro-, micro- and nanoscopic). The contact angle is, in most cases, measured directly after processing or the measurement time point is not specifically defined [9-14]. It is assumed that the contact angle is stable, and its value does not change. In the past 10 years various publications have reported that the wettability of surface structures (like LIPSS) can be time-dependent [4,15-17].

This article elaborates on experimental investigations on the changing wettability of technical ceramics (aluminum oxide and nitride). Two different microstructures are realized as pillar structure and hole structure by means of a picosecond laser in order to specifically change the wettability of the surface. The measurement time point of the water contact angle (WCA) after processing is included for the analysis and evaluation. Theoretical models after Wenzel and Cassie-Baxter are applied to describe the experiments.

The approach is used to create surface structures in the micrometer range on ceramic printed circuit boards. Thus, specific characteristic changes in terms of substrate wettability can be caused in order to e.g., guide or stop fluidic during chip placement and joining.

## Material and Methods

Aluminum oxide ($Al_2O_3$) and aluminum nitride substrates (AlN) are processed for the experiments by means of laser pulses in the picosecond range with different laser parameters. The materials have an initial roughness of Ra = 0.32 µm, which is determined using the stylus instrument "Form TalySurf Series 2" from TAYLOR HOBSON. The contact angle of the initial surface of aluminum nitride is 84° ± 4° and of aluminum oxide 52° ± 3°. The used laser is

the "TruMicro 5050" provided by the company TRUMPF, which is an ultrashort pulse laser with a pulse duration of <10 ps and pulse energies of up to 250 µJ. Yb:YAG serves as pump medium for the disc laser amplifier. The processing wavelength of the laser is 1030 nm and the repetition rate determined constant for all experiments is set at 25 kHz. The output beam diameter of 4.5 mm is coupled into the scanning system "HurrySCAN II 14". This system from the company SCANLAB is equipped with two galvanometer mirrors and an F-Theta lens with a focal length of 100 mm. The scan field size results from the used lens and provides a possible processing area of 60 x 60 mm$^2$. An XY stage from the company STEINMEYER enables a processing of substrates which exceed the scan field. The contact angle is applied in order to illustrate the wetting behavior of surfaces. The contact angle measuring device "OCA 15 Plus" from DATAPHYSICS is used for the examinations. The four µl droplets of distilled water were applied to the laser-processed surface structures under atmospheric conditions. The static contact angle is calculated through analyses of droplet images which are acquired directly after the droplet separation. Further surface analyses as well as a characterization of the structure sizes after processing are carried out by means of the laser scanning microscope "VK-X100" from KEYENCE. All samples were stored in plastic boxes with microfiber cloths and plastic foam for stabilization reasons.

For clarification, Figure 1 shows the cross section (top) and the top view (bottom) of such structures which are generated. Figure 1 contains the structure size *a*, the structure distance *b*, the structure height *H*. For the hole structure a and b are inverted. The decision for the square shape of the final structures was made based on the observations in publications [9] and [11]. So, there are no significant differences between square and round shapes.

| | Wenzel | | Cassie | |
|---|---|---|---|---|
| **General** | $\cos\theta_{WE} = r \cdot \cos\theta$ | (1) | $\cos\theta_{CB} = \varphi(\cos\theta + 1) - 1$ | (5) |
| with | $r = \frac{A_{real}}{A_{projeziert}}$ | (2) | $\varphi = \frac{1}{(b/a + 1)^2}$ | (6) |
| | $A_{real} = (a+b)^2$ | (3) | | |
| | $A_{projeziert} = (a+b)^2 - (b^2)$ | (4) | | |
| **Square shape** | $\cos\theta_{WE} = (1 + \frac{4A}{a/H})\cos\theta_0$ | (7) | $\cos\theta_{CB} = \varphi(1 + \cos\theta_0) - 1$ | (8) |
| **Round shape** | $\cos\theta_{WE} = (1 + \frac{\pi DH}{b^2})\cos\theta_0$ | (9) | $\cos\theta_{CB} = \frac{\pi D^2}{4b^2}(\cos\theta_0 + 1) - 1$ | (10) |

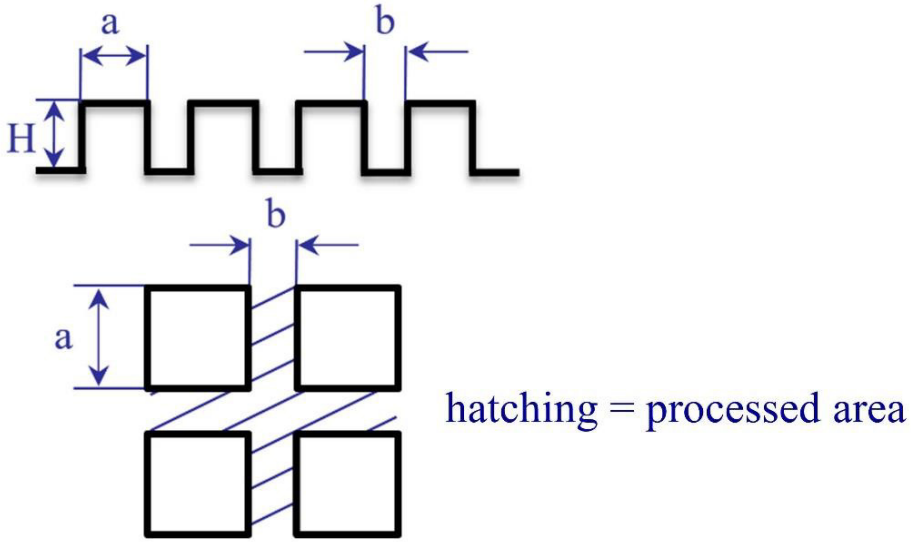


**Figure 1:** Schematic cross (above) and top view (bottom) section illustration of the square pillar structure.

Table 1 shows how the microstructures were realized with a spacing factor varying from 0.15 to 1.80. The structure sizes and distances were determined and extended by means of the state of the art.

**Table 1:** Spacing factors, structure sizes, distances for the experiments.

| Spacing Factor, *b/a* | Structure Size, *a* | Structure Distance, *b* |
|---|---|---|
| 0.15 | 200 | 30 |
| 0.3 | 100 | 30 |
| 0.3 | 200 | 60 |
| 0.45 | 200 | 90 |
| 0.6 | 50 | 30 |
| 0.6 | 100 | 60 |
| 0.9 | 100 | 90 |
| 1.2 | 50 | 60 |
| 1.8 | 50 | 90 |

Table 2 lists the different parameter combinations for the desired spacing factors of holes and pillars, generated by means of a picosecond laser. The list results from an extensive parameter study to keep the structure height *H* constant for all experiments.

**Table 2:** Experiment plan for laser structuring at constant 25 kHz.

| Material | Structure | Over Scans | Pulse Distance | Fluence |
|---|---|---|---|---|
| AlN | Pillar and hole | 5 | 2,5 | 8 |
| | | 10 | | |
| | | 5 | 5 | 10 |
| | | 10 | | |
| $Al_2O_3$ | Pillar | 5 | 10 | 6 |
| | | 10 | | |
| | | 5 | 15 | |
| | | 10 | | |
| | Hole | 2 | 2,5 | 4 |
| | | 4 | | |
| | | 2 | 5 | |
| | | 4 | | |

The scanning speed and fluence had to be adjusted for the material $Al_2O_3$ so that *a*, *b*, *H* could be carried out constant to AlN due to the different material characteristics such as density and band gap.

First and foremost, the selected parameters and structures are to cause a change of the wetting behavior of the material surfaces. In addition to that, the results are to be correlated with the following-described models of Wenzel and Cassie-Baxter.

## Theory and Calculation

To make a statement on the contact angle, it can be deduced from different models based on the Young equation, named after *Thomas Young* [18]. For this the parameters *a*, *b*, *H* are determined and included in the calculation. The calculation of the theoretical angle is based on the following equations according to [2,6,19]:

A stand for the surface ratio between real surface and projected area and $\theta_0$ for the initial water contact angle.

In order to obtain an overview of the behavior of both models depending on different structuring procedures materials, and data on *a*, *b*, *H* and $\theta_0$ are collected from numerous publications. The data for the calculation (see Table 3) applying formulas 7 and 8 are taken from the references.

**Table 3:** Overview of the state of the art – Structuring.

| Technology | Material | Structure | Shape | a [µm] | b [µm] | H [µm] | Source |
|---|---|---|---|---|---|---|---|
| Lithography | PDMS | pillar | square | 25 | 8-80 | 30 | [2] |
| Lithography & ICP | Si | pillar | square | 10-85 | 5-30 | 15 | [6] |
| Anodization | $Al_2O_3$ | hole | round | 0.085 - 0.42 | 0.03 - 0.365 | 4.5 | [10] |
| Lithography | SU8 Photoresist | pillar, hole | square | 20 | 10-45 | 30 | [7] |
| DMDCS coated | Si | pillar | square, round | 8 - 100 | 5-35 | 30 - 32 | [9] |
| Etching | AAO | hole | round | 0.141 - 0.354 | 0.043 - 0.264 | 7.9 | [8] |
| Laser | Co-Cr-Mo | hole | square, round | 50 - 150 | 100 - 300 | 8-16 | [11] |
| Laser | Al6061 | pillar | square | 50 - 300 | 5 | 5 | [12] |
| Laser | PDMS | pillar | square | 300 - 4800 | 200 | 10 | [13] |
| Laser | $SiO_2$, Polystyrene | pillar, hole, LIPSS | square | 10 | 10 | 5.3 | [3] |
| Laser | Al 99.999% | pillar | square | 200 | 5 | 19 | [14] |

Figure 2 shows the experimental raw values without any modification taken from the publications for the later comparison of the theoretical graphs. The data exhibit a different distribution of the contact angle depending on the material and technology.

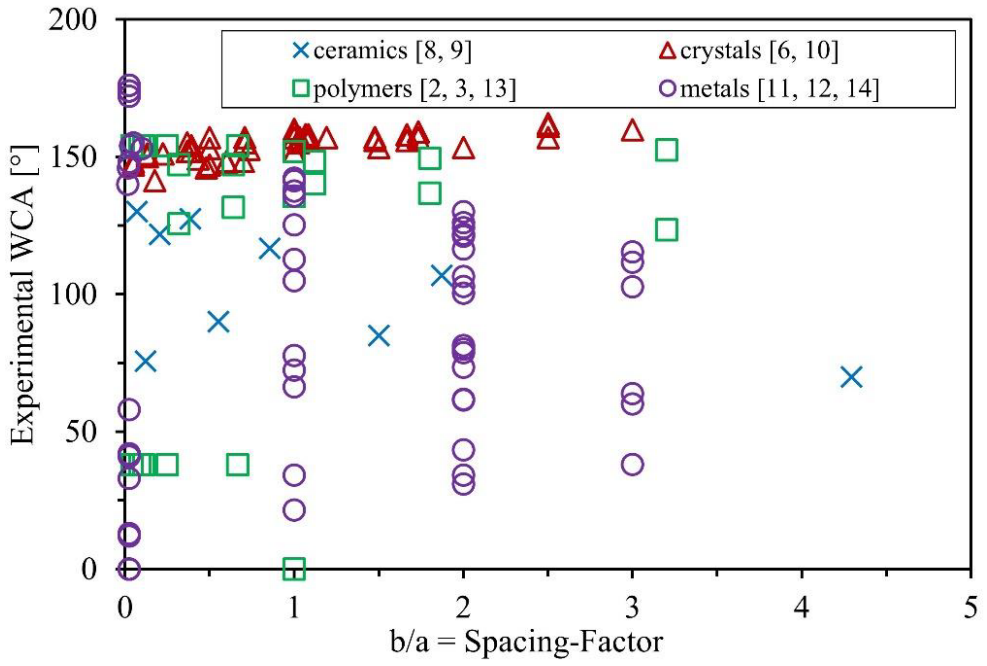


**Figure 2:** Experimental WCA depending on b/a taken from the publications [2,3,6,8-14].

Figure 3 and Figure 4 summarize the calculated theoretical WCA according to the models of Wenzel (formula 7) and Cassie-Baxter (formula 8) from different literature to proof the behavior. The initial contact angle of the unprocessed output surface is incorporated into the theoretical calculation and must therefore be given from the reference. The following graphs give an overview of the theoretically calculated curve according to the different sources, which enables a first evaluation of the models by means of existing experimental data on *a*, *b*, *H* and $\theta_0$. Furthermore, the sources contain different structuring procedures which are not necessarily based on lasers as well as numerous materials which are divided into four groups. Most publications compare the contact angle with the spacing factor in order to illustrate the influence of a varying structure size. The spacing factor results from relation between structure distance and structure size.

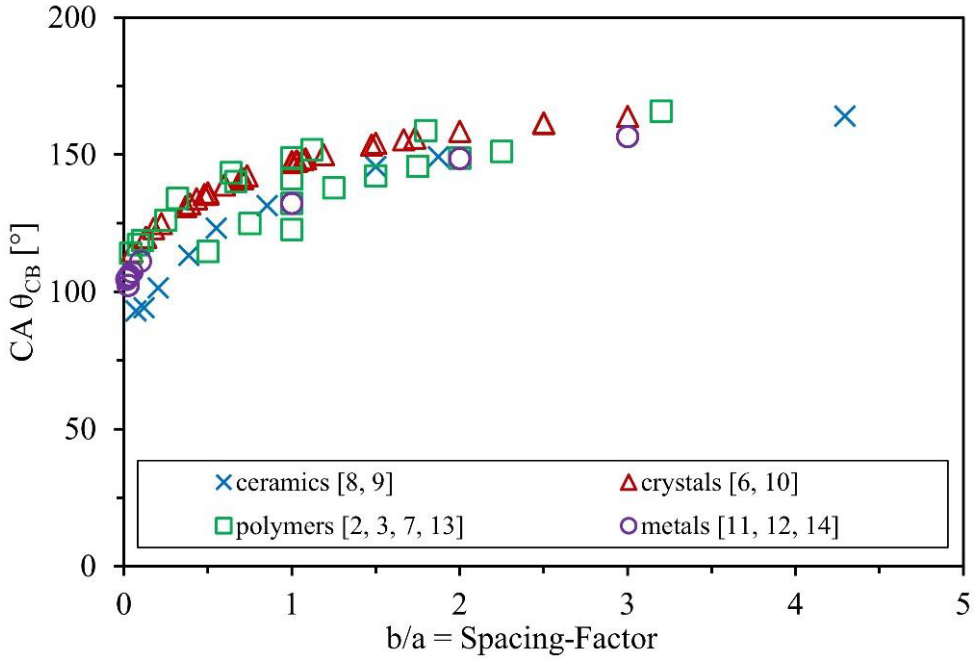


**Figure 3:** Theoretical CA depending on b/a according to the Cassie-Baxter model (formula 8) [2,3,6-14].

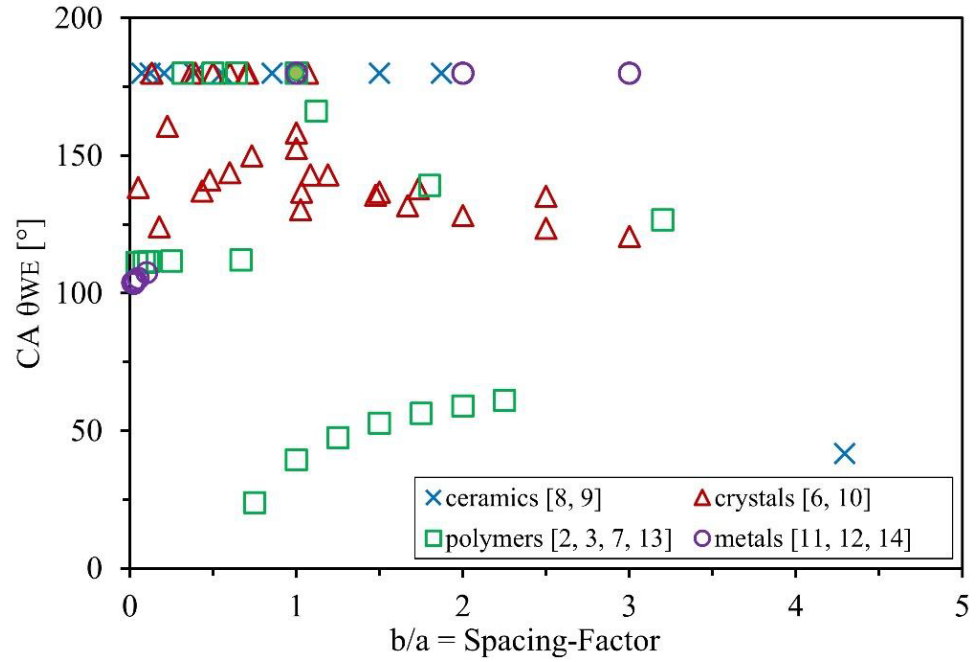


**Figure 4:** Theoretical CA depending on b/a according to Wenzel's model (formula 7) [2,3,6-14].

Figure 3 compares the contact angles and the spacing factor according to Cassie-Baxter. The height of the structures is not part of the calculation of the theoretical contact angle because, according to this model, air pockets develop between the structures which makes high contact angles necessary, see Figure 3. Based on this equation, the data points allow an independent comparison as the structure height *H* has no influence. According to the Cassie-Baxter model, the contact angle increases as the spacing factor rises. This is true no matter what materials are used and agrees well with the model curve. Furthermore, it is obvious that in many publications the theoretical superhydrophobic contact angle is reached when the spacing factor is ca. "1.5". According to most sources, the superhydrophobic contact angle begins at a contact angle between 140 and 150° [1,3,5,11,12].

Figure 4 shows that the majority of the contact angles calculated according to Wenzel's model is in the hydrophobic or superhydrophobic range. The data in the publications of He et. al. and Ran et. al. indicate a decreasing contact angle with an increasing spacing factor [2,9]. The calculated values show that numerous superhydrophobic contact angles develop [8]. It is obvious that with a decreasing spacing factor the contact angle can decrease as well, as illustrated by Priest et. al. [7]. The sources most precisely investigate the range "*b/a*" between zero and one. The publication of Zhu et. al. shows another possible course of the curve, where the spacing factor increases up to *b/a* = 1 with a simultaneously increasing contact angle. Following this the contact angle goes down to *b/a* = 3 [6]. Figure 4 indicates that the spacing factor alone does not correlate completely with Wenzel's model regardless of the material, chemical composition and, if necessary, laser parameters. The height *H* of the structures is included in the calculation of the contact angle according to Wenzel, which is an additional compared with Cassie-Baxter.

Figures 3 and 4 show that both models are suitable for the calculation of the theoretical curve, which has to be compared subsequently with the experimental data in order to check the congruence with the model. Furthermore, it is obvious that not only the spacing factor influences the wettability, but many other parameters (material, procedures) have an impact on it and limit these model approaches.

The following sub-chapter elaborates on the influence of the contact angle in relation to the time factor so that a combination of both factors (structural parameters and time) constitutes a possible extension. The data are also taken from different references and summarized.

Figure 5 shows the time dependence of experimentally determined contact angles and their respective materials. This illustrates the fact that, after processing, different materials and their measurement time point have effects on the contact angle and thus the wetting behavior of structured materials. The Y-axis represents the defined contact angle, and the X-axis represents the time in days. All sources in figure 5 use short laser pulses (ns to fs) and the infrared wavelength range.

The publication of Bizi-Bandoki describes experiments in which stainless steel is roughened by means of a pulsed fs-laser. Furthermore, it explains that, in the course of time, there is a change from hydrophilicity to hydrophobicity which is a result of the modifications of the surface chemistry. Different pulse distances (5, 10, 15 & 20 µm) are used and the measurements are carried out from day 0 to day 8 after processing. Figure 5 reveals that the determined contact angles of 27° on day 1 steadily rise to maximal 132° on day 5 after processing [15].

The publication of Li illustrates over a long period of up to 30 days the increase of the contact angle of ca. 78° (after processing) up to ca. 130°. This process creates lines, pillars and holes in a titanium alloy by means of a pulsed ns-laser. Figure 5 exclusively describes the measurement results for a pillar structure with structure sizes of 50 and 100 µm. The contact angle decreased with both structure sizes after the first day of processing to 25° and increased afterwards steadily. So, this publication describes that the change from hydrophilicity to hydrophobicity is connected with the surface structure. It has been shown that the increased carbon content of Ti-6Al-4V is responsible for the hydrophobic behavior which could be observed on the surface [1].

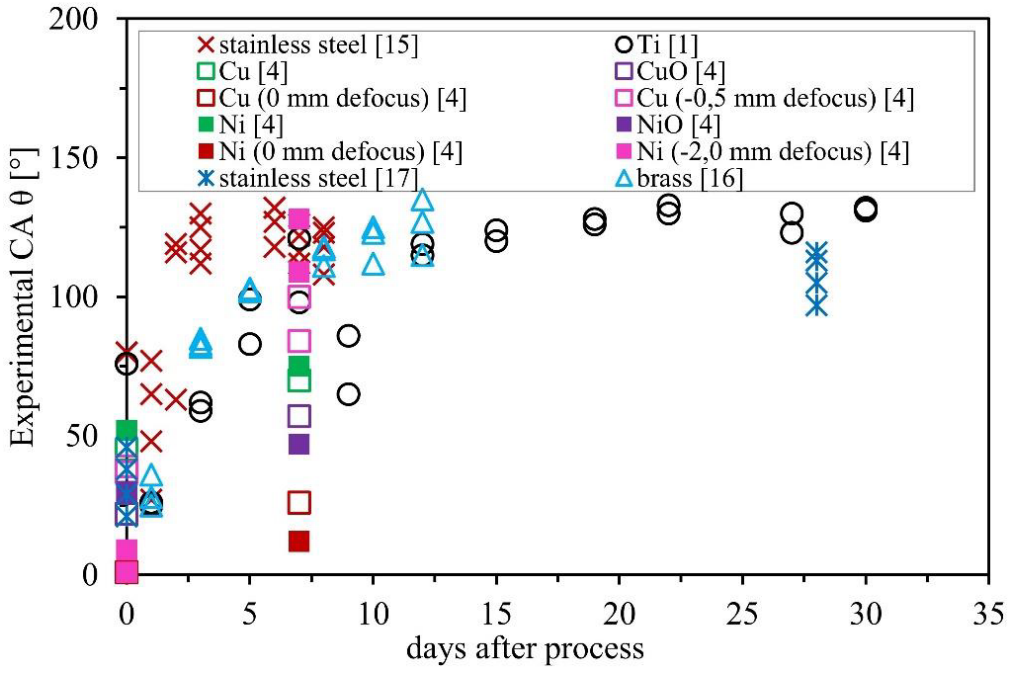


**Figure 5:** Experimental CA in relation to time from important publications and their materials [1,4,15-17].

In the year 2016 Zhang describes a wide range of results for the time dependence of the contact angle for different materials and process settings. Copper (Cu) and Nickel (Ni) were investigated with different focal positions (0, -0.5 and -2 mm) as well as CuO and NiO. The LIPSS structure is realized through the line focusing of a femtosecond laser with low repetition rate (1 kHz) using a cylindrical lens. The surface structures were changed through optimizing the defocusing distance and the scanning speed. The contact angles are measured from day 0 to day 7 after processing. Irrespectively of the material and the parameter setting, the contact angles determined in this publication range from 1° (directly after processing) to 128° on the 7th day of measurement. A strongly time-dependent water contact angle could be determined with both materials. The chemical surface analysis showed that the absorption of hydrophobic functional groups changed the surface from wetting in the Wenzel state to wetting in the Cassie state, which was responsible for the transition from hydrophilic to hydrophobic. Compared to our measurement results, clear rises of the contact angles after a short time can be recognized. The publication always provides results shortly after processing and after 7 days where we can recognize slight rises, as with Ni (0 mm defocus) on the one hand, as well as sharp rises, as with Ni (-2.0 mm defocus) on the other hand. Ni (0 mm defocus) had the lowest impact on time with a contact angle of 1° on the first day of measurement and a contact angle of 12° on the 7th day. Ni (-2.0 mm defocus) has the highest rise of the contact angle from 9° (1st measurement day) to 128° (7th measurement day) [4].

Rung's publication from the year 2018 shows contact angle measurements directly and 28 days after processing. LIPSS structures are created on stainless steel (X5CrNi18-10) by means of a pulsed fs-laser using different fluences (0.2; 0.4; 0.6 & 0.8 J/cm$^2$). The narrowest contact angle of 21° (day 0) and the widest contact angle of 116° (day 28) are reached with a fluence of 0.8 J/cm$^2$. The publication summarizes that the laser fluence and pulse overlapping influence the wettability, which is described by the static contact angle, the time-dependent contact angle as well as the contact angle hysteresis in a complex way. The measurements 28 days after processing show a hydrophobic behavior with a static contact angle of over 97° [17].

In another publication of Rung contact angle measurements are described from one day and twelve days after processing, where a LIPSS structure is created in brass by means of a pulsed femtosecond laser. Again, different fluences (0.87; 1.63; 1.96 J/cm$^2$) are used. In summary it is concluded that changing the surface structure additionally influences the wetting behavior. Especially raising the fluence and pulse overlapping lead to narrower contact angles directly after processing and to wider contact angles after a time period of 12 days [16].

The data from the used sources all in all indicate a rise of the contact angle depending on the measurement time point. The maximal contact angle is reached at different time points after processing. In [15] the maximum contact angle with stainless steel is already partly reached on day 3. Other sources, however, illustrate a slighter steady rise [1,17].

The data in Figure 5 exclusively contain metallic materials which have a LIPSS structure or a surface roughening. LIPSS structures, however, are only to a certain extent suitable to calculate the theoretical contact angle with the referred models as the necessary structure sizes are difficult to analyze. They have not been compared yet using the above-mentioned two models.

This publication is aimed at investigating the time dependence of the contact angle of ceramic materials and the correlation with the existing models. For this, microstructures are created by means of direct laser structuring and examined for a time-dependent contact angle. The different models for the description of the contact angle partly contradict each other and are to be examined for the technical ceramics used in the paper. Furthermore, the time-dependent contact angle is to be examined for the technical ceramics in comparison to results from literature where only metallic materials and roughening/LIPSS have been examined so far.

## Result and Discussion

The following part presents the results of the structuring and contact angle analysis. The diagrams show the influence of spacing factor and time dependence of the contact angle. The trendlines in the diagrams portray the theoretical courses for the respective pillar and hole structures according to the models of Wenzel (formula 7) and Cassie-Baxter (formula 8). The measured output angles of both ceramics are applied for the calculation.

Figure 6 compares the measured contact angle values of the squared pillar structures with the spacing factor. The theoretical trend lines according to Wenzel and Cassie-Baxter for the respective materials originate from formulas 7 and 8. The measurement values of $Al_2O_3$ exhibit a slight decrease up to the 7th day with a spacing factor 0.6. The development of the measurement values on the 7th day of measurement correlates with the theoretical values according to Wenzel. This behavior is also true for the first two measurement days with an offset. The behavior according to Wenzel generally describes the first measurement days of both ceramics with a narrower contact angle better than later superhydrophobic values.

Contact angles from 0° to ca. 82° are reached up to the 7th measurement day. The superhydrophobic contact angles, no matter which set of parameters from Table 2 was applied, can be recognized 250 days after processing. The contact angles after 250 days determined in the experiments range from ca. 125° up to ca. 145°.

The diagram in figure 6 (right) shows the measurement data of the pillar structures of aluminum nitride determined in the experiments. It is obvious that on the first three measurement days the surfaces lead to hydrophilic or super hydrophilic contact angles. The measurement values show a course which is similar to the theoretical curve according to Wenzel, however, with a clear offset of ca. 70°. The determined contact angles range from 0° to ca. 17°. The widest recognizable contact angle up to the 7th day of measurement for AlN in Figure 6 (right) is 17.62° which is reached with a structure size of 100 µm and a structure distance of 90 µm. It is also obvious that, except for few values, the surface of AlN is super hydrophilic directly after the processing. Thus, the selected laser

parameter set has no impact on the surface wettability. 250 days after processing, two groups can be recognized, with AlN a little more clearly than with $Al_2O_3$. The first group of the 250th measurement day for the material AlN shows contact angles of around 80°, which can be compared with the theoretical contact angles according to Wenzel's model. The second group, however, shows contact angles of around 140° and can be compared with the theoretical contact angle according to the model of Cassie-Baxter.

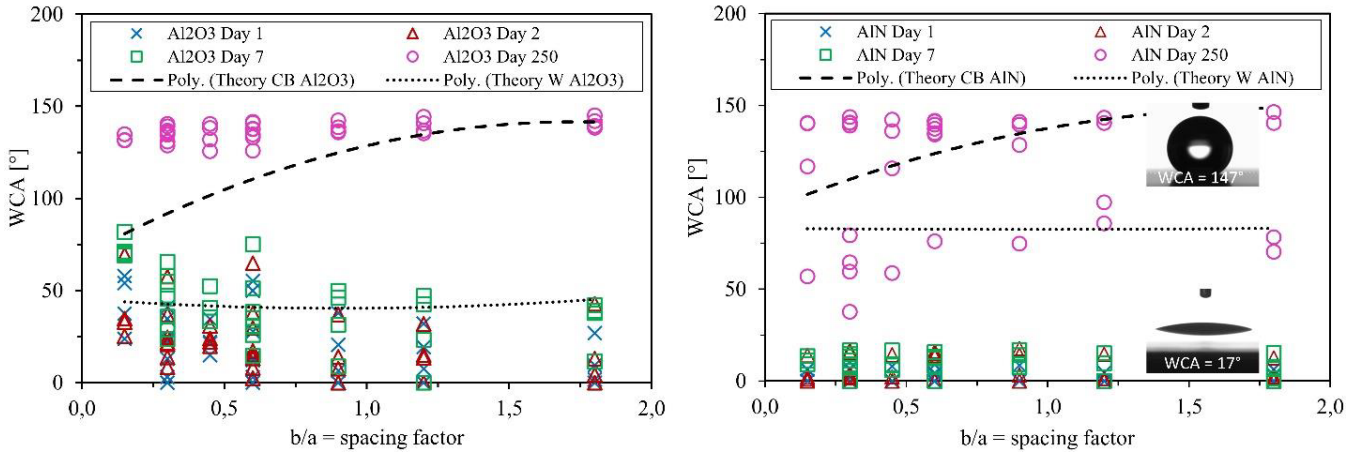


**Figure 6:** WCA of the pillar structure $Al_2O_3$ (left) and AlN (right) depending on spacing factor and time (theoretical Fits of Cassie-Baxter (dashed, [formula 8]) and of Wenzel (dotted, [formula 7])).

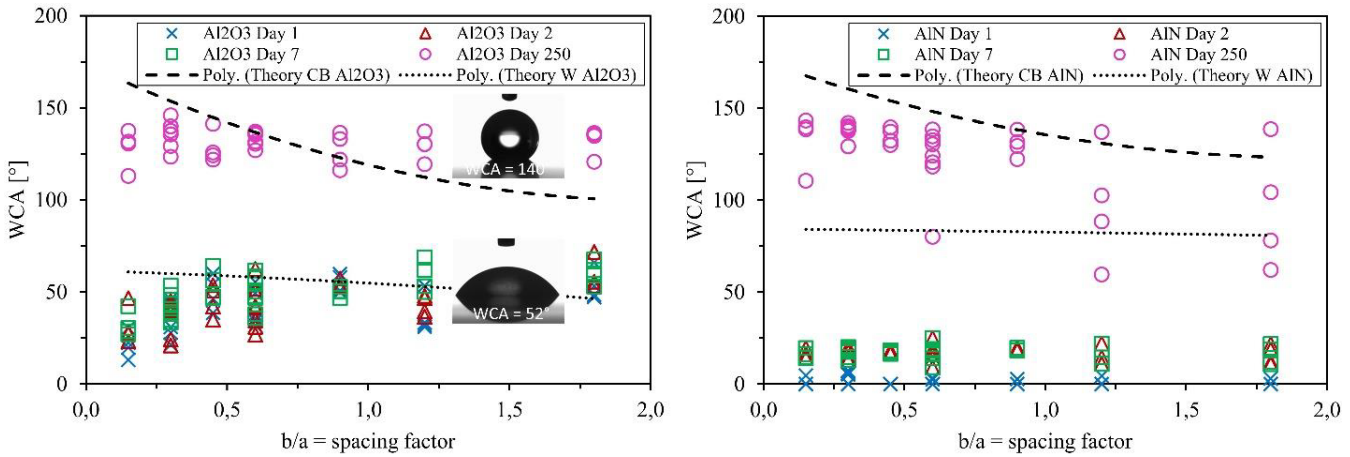


**Figure 7:** Hole structure $Al_2O_3$ (left) and AlN (right) determined WCA depending on the spacing factor and time (theoretical Fits of Cassie-Baxter (dashed, [formula 8]) and of Wenzel (dotted, [formula 7])).

In contrast to the state of the art, no significant rises of the contact angles can be recognized with the used ceramics after few days. If you furthermore compare the measurement values of the ceramics with the previously described publications, it can be recognized that, after a certain period of time, a wide contact angle can be reached (>140°). The publication of Li et. al. proves this effect with metals as the superhydrophobic status is reached after ca. 23 days [1]. Comparable tendencies towards time dependence of the contact angle and the $Al_2O_3$ as well as the AlN can be recognized in the publication of Zhang et. al. So, partly the contact angle of copper is θ = 1° directly after the structuring and 7 days after structuring already θ = 26° [4].

In Figure 7 the contact angle measurement values of the different measurement days are compared with the spacing factor. No hydrophobic contact angles can be measured until the 7th day of measurement for both ceramics. It can be recognized that the contact angle of $Al_2O_3$ increases slightly with an increasing spacing factor. Until the 7th day of measurement, the measurement values of $Al_2O_3$ range from ca. 15° to 70° depending on the used parameter set. Thus, the surface becomes more hydrophobic with an increasing spacing factor. A similar course for hole structures can be found in the publication of Ran et. al. see Figure 2 [9]. $Al_2O_3$ is also used in the experiments of this publication and with an increasing spacing factor wide contact angles are achieved. Again, an overlapping of the

$Al_2O_3$ values with the theoretical values according to Wenzel can be seen. This enables a directed change of the surface wettability. The widest recognizable contact angle for $Al_2O_3$ until the 7th day of measurement is 68.77°, which is reached with a structure size of 50µm and a structure distance of 60µm. Furthermore, five over scans and a pulse distance of *dp* = 15µm are necessary to reach this value. It is obvious that for the creation of a hole structure with wide contact angle only a small number of passages is required.

Contact angle values were determined again 250 days after processing, which showed that the values determined in the experiments are similar to the theoretical values according to Cassie-Baxter. No matter which parameter set was used, contact angle values between ca. 113° - 146° could be achieved after 250 days.

According to the theoretical curves, there is no decrease recognizable for the measured contact angles of the hole structure. Li's publication from 2015 provides similar results where the contact angle for a structure with a structure distance of 50 µm increases from 26° (first day) up to 132° (30th day).

Figure 7 (right) compares, as with the pillar structure, the contact angle values of AlN with the spacing factor for the hole structure exhibiting various effects again. Again, there is an offset recognizable between the trendlines of AlN and the one according to Wenzel, however with a smaller offset of ca. 64°. Both trendlines have similar courses, not depending on the increasing spacing factor. As with the pillar structure, the measurement values of AlN are less diversified than the measurement values of $Al_2O_3$. Depending on the used parameter set, the measurement values range from ca. 0° - 25° until day 7 of measurement.

The widest contact angle (25.00°) for AlN is reached with a structure size of 50 µm and a structure distance of 30 µm. The pulse distance here is *dp* = 5 µm and the number of over scans *N* = 5. A comparison of the determined results on AlN is based on the publication of Zhang et. al., as it also shows an increase of the contact angle on copper by ca. 25° (1° → 26°) within seven days. An almost similar rise of the contact angle can be observed with isolated $Al_2O_3$ measurement data. So, the contact angle on $Al_2O_3$ increases after seven days by ca. 35° (22° → 57°), similar to Zhang's publication from 2016 (material CuO) [4].

250 days after processing, hydrophilic contact angles (<90°) and hydrophobic to superhydrophobic contact angles can partly be recognized, which again overlaps with Wenzel's and Cassie-Baxter's models. Contact angles of ca. 59° to ca. 143° can be determined on the 250th day of measurement. In the experiments with $Al_2O_3$ the contact angle increases from 22° to 132° within 250 days. The results of Rung et. al., where the contact angle increases from 21° (day 1) to 116° (day 28), confirm the trend that the contact angles rise with increasing storage time [17]. Furthermore, the results of AlN represent an equivalent to the results of Zhang et. al. (material Nickel). So, directly after processing a super hydrophilic contact angle of 1° can be observed which increases to a hydrophobic contact angle of 109° after seven days [4] (Table 4).

**Table 4:** Overview – average contact angles of both ceramics.

| | AlN | | $Al_2O$ | |
|---|---|---|---|---|
| | **Average Contact Angle Day 1-7** | **Average Contact Angle Day 250** | **Average Contact Angle Day 1-7** | **Average Contact Angle Day 250** |
| Pillar | 5.96 | 115.15 | 28.48 | 136.71 |
| Hole | 8.33 | 123.29 | 44.72 | 131.54 |

If you compare the measuring values with those from the above-described publications, you can see that the contact angle can become superhydrophobic after a certain time. This effect is very obvious in the publication of Li et. al. [1] and the superhydrophobic status is reached after ca. 23 days. The publication of Rung et. al. reveals similar tendencies whereas this effect is measurable after 28 days [17].

## Conclusion

Ceramic substrates of aluminum oxide ($Al_2O_3$) and aluminum nitride (AlN) were structured by means of ultrashort laser pulses and their wetting characteristics were specifically set. For this, the time-dependent wettability of pillar and hole structures is examined. The influence of the spacing factor and the storage time is included in the examinations.

The influence of the storage time on the examined samples is not very high after few days. For this period of time, it can be clearly recognized that the measurement values of $Al_2O_3$ vary more than those of AlN.

It can be summarized that 250 days after processing superhydrophobic contact angles can be determined with both materials. They develop especially with $Al_2O_3$ no matter which parameter set is selected. With AlN hydrophilic contact angles can be partly found even after 250 days. The determined measurement data after 250 days of both materials can be compared with the described publications as they prove that after a certain time a hydrophobic contact angle develops.

Furthermore, the direct structuring of technical ceramics by means of ultrashort laser pulses is a highly suitable procedure for manufacturing microstructures. In any case, the influence of the storage time of the materials on the contact angle should be taken into consideration. The determined results are partly acknowledged by literature. However, the different material characteristics (metals - ceramics) and structure forming procedures (LIPSS - pillar and hole) should not be neglected.

Based on the gained findings, it is possible to transfer the manufactured structures to a chip layout in order to create a flow limit (marked red) and prevent the liquid used to glue (Delo-Monopox) the chips. This implies that the bond areas must not get dirty and thus a through connection, or a faulty wiring can be prevented, see Figure 8.

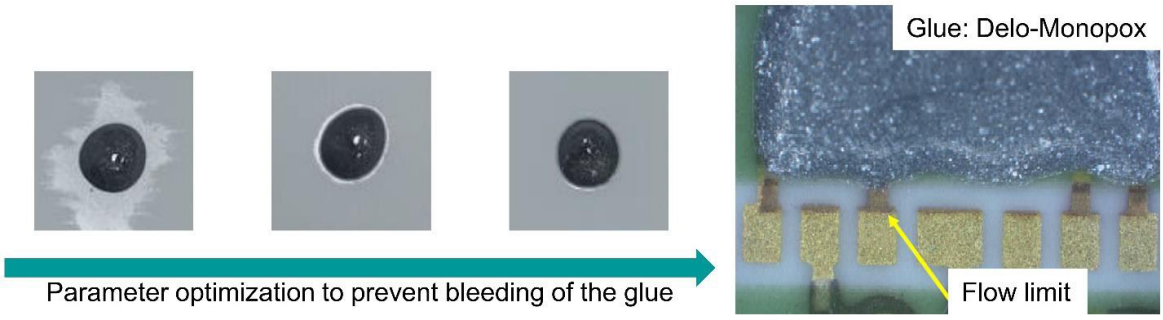


**Figure 8:** Optimization of parameters (left) and Chip layout with flow limit & glue (right).

## Acknowledgement

We especially want to thank LUST Hybrid-Technik GmbH for the experimental investigations on the chip layout.

## Funding

This work was supported by the federal state of Thuringia within the framework of the joint project "ProFunk" (2015 VF 0021).

## Conflict of Interest

The authors declare no conflict of interest.

## Reference

1. Y Li, Y Tian, C Yang, D Zhang, X Liu (2015) The 5th International Conference on Manipulation, Manufacturing and Measurement on the Nanoscale: 5-9 October 2015, Changchun, China conference proceedings, IEEE, Piscataway, NJ, pp. 153-158.
2. B He, NA Patankar, J Lee (2003) Multiple Equilibrium Droplet Shapes and Design Criterion for Rough Hydrophobic Surfaces. Langmuir 19(12): 4999-5003.
3. C Kunz, FA Müller, S Gräf (2018) Multifunctional Hierarchical Surface Structures by Femtosecond Laser Processing. Materials (Basel) 11(5): 789.
4. Y Zhang, G Zou, L Liu, Y Zhao, Q Liang, et al. (2016) Time-dependent wettability of nano-patterned surfaces fabricated by femtosecond laser with high efficiency. Applied Surface Science 389: 554-559.
5. R Jagdheesh (2014) Fabrication of a superhydrophobic $Al_2O_3$ surface using picosecond laser pulses. Langmuir 30(40): 12067-12073.
6. L Zhu, Y Feng, X Ye, Z Zhou (2006) Tuning wettability and getting superhydrophobic surface by controlling surface roughness with well-designed microstructures. Sensors and Actuators A: Physical 130-131: 595-600.
7. C Priest, TWJ Albrecht, R Sedev, J Ralston (2009) Asymmetric wetting hysteresis on hydrophobic microstructured surfaces. Langmuir 25(10): 5655-5660.
8. JG Buijnsters, R Zhong, N Tsyntsaru, JP Celis (2013) Surface wettability of macroporous anodized aluminum oxide. ACS Appl Mater Interfaces 5(8): 3224-3233.
9. C Ran, G Ding, W Liu, Y Deng, W Hou (2008) Wetting on nanoporous alumina surface: transition between Wenzel and Cassie states controlled by surface structure. Langmuir 24(18): 9952-9955.
10. CE Cansoy, HY Erbil, O Akar, T Akin (2011) Effect of pattern size and geometry on the use of Cassie–Baxter equation for superhydrophobic surfaces, Colloids and Surfaces A: Physicochemical and Engineering Aspects 386(1-3): 116-124.
11. L Qin, P Lin, Y Zhang, G Dong, Q Zeng (2013) Influence of surface wettability on the tribological properties of laser textured Co–Cr–Mo alloy in aqueous bovine serum albumin solution. Applied Surface Science 268: 79-86.
12. DM Chun, G Davaasuren, CV Ngo, CS Kim, GY Lee, et al. (2014) Fabrication of transparent superhydrophobic surface on thermoplastic polymer using laser beam machining and compression molding for mass production. CIRP Annals 63(1): 525-528.
13. B Farshchian, JR Gatabi, SM Bernick, S Park, GH Lee, et al. (2017) Laser-induced superhydrophobic grid patterns on PDMS for droplet arrays formation. Applied Surface Science 396: 359-365.
14. CV Ngo, DM Chun (2018) Control of laser-ablated aluminum surface wettability to superhydrophobic or superhydrophilic through simple heat treatment or water boiling post-processing. Applied Surface Science 435: 974-982.
15. P Bizi-bandoki, S Valette, E Audouard, S Benayoun (2013) Time dependency of the hydrophilicity and hydrophobicity of metallic alloys subjected to femtosecond laser irradiations. Applied Surface Science 273: 399-407.
16. S Rung, S Schwarz, B Götzendorfer, C Esen, R Hellmann (2018) Time Dependence of Wetting Behavior Upon Applying Hierarchic Nano-Micro Periodic Surface Structures on Brass Using Ultra Short Laser Pulses. Applied Sciences 8(5): 1-13.
17. S Rung, S Schwarz, B Götzendorfer, C Esen, R Hellmann (2018) Static and Dynamic Contact Angle of Water Influenced by Femtosecond Laser Based Ripple Structures on Metals. JLMN 13(2): 100-104.
18. T Young (1805) III. An essay on the cohesion of fluids. Phil Trans R Soc 95: 65-87.
19. NA Patankar (2003) On the Modeling of Hydrophobic Contact Angles on Rough Surfaces. Langmuir 19(4): 1249-1253.